 doi:10.20944/preprints202210.0047.v1

Article

Correlating the Macrostructural Variations of an Ion Gel with Its Carbon Dioxide Sorption Capacity

Tung Nguyen, Mona Bavarian, and Siamak Nejati *

Department of Chemical and Biomolecular Engineering, University of Nebraska-Lincoln

* Correspondence: snejati2@unl.edu

Abstract: We report on a direct correlation between macroscale structural variations and the gas sorption capacities of an ion gel. Here, we chose 1-ethyl-3-methylimidazolium bis(trifluoromethyl sulfonyl)imide ([Emim][TF_2N]) and poly(vinylidene fluoride)-co-hexafluoropropylene (PVDF-HFP) as the ionic liquid and host polymer, respectively. The CO_2 sorption in the thin films of IL-polymer was measured by the gravimetric method. The results of our experiment show that the trend of CO_2 uptake of these mixtures is non-linearly correlated with the content of IL. Here we highlight the variation in the molecular structure of the polymers is the main reason behind the observed trend. The presented data suggest the possibility of using the composition of mixtures containing IL and polymers to realize a synergistic gain for gas sorption in these mixtures.

Keywords: Gas sorption; polymer; ionic liquids; carbon dioxide; synergy

1. Introduction

Macromolecules and their mixtures are essential for the development of medias used in membrane-based separation. Among various polymer mixtures, those containing ionic liquids (ILs) present an interesting class of materials with many applications.[1] Over the past two decades, many studies have been devoted to investigate the properties of these mixtures.[2–4] Because ILs are widely explored as reversible CO_2 absorbents, and their mixtures have been considered selective solvents for CO_2 sorption,[5,6] polymeric membranes containing ILs gained substantial attention.[7] In the simplest form, mixing ILs with polymers and casting films from these mixtures led to the development of membranes, referred to as supported ionic liquid membranes (SILMs)[8,9] .

The use of ILs within polymeric domains was first explored for developing ionogels[10] and later in SILM systems.[11] Using PVDF-based SILM for CO_2 separation, it was observed that the solubility of CO_2 in SILM could be improved two fold when compared with that of ILs.[12] By confining ILs in a lyotropic liquid crystal, a similar observation was made.[13] The above observations point to the possibility of tuning gas sorption capacities in IL phases by mixing ILs with complex fluids. Classical theory suggests that preparing such mixtures can lead to the reduction of the cohesive forces of the IL phase, and reduce the required energy for forming a cavity for the guest gas molecules.[14] Additionally, ordering the ILs close to a solid wall is frequently reported and is thought to be the explanation for the enhanced solubility of gas in IL in confinement.[15–20]

Herein, we report on the significance of the composition of a well-known polymer gel, composed of poly (vinylidene fluoride-co-hexafluoropropylene) and 1-ethyl-3-methylimidazolium bis(trifluoromethyl sulfonyl)imide, on their CO_2 sorption capacities. We note that swelling of polymers and configuration changes that lead to the structural variation of polymers are responsible for the observation of 1.5-fold enhancement in CO_2 sorption in these mixtures. By controlling the composition of the mixture, we demonstrate a

 doi:10.20944/preprints202210.0047.v1

clear macrostructure-to-function relationship for CO_2 solubility in these mixtures. Utilizing carbon-based additives as nucleating agents, we further explore the role of crystallinity and structure of the samples on CO_2 sorption. The results suggest that the suppression of β-phase in polymer has a pronounced effect on the CO_2 sorption capacity of the samples.

2. Materials and Experiments

2.1. Materials

Imidazolium-based Ionic Liquids, 1-ethyl-3-methylimidazolium bis(trifluoromethyl sulfonyl)imide ([Emim][TF_2N]) with a purity of ≥ 98%, Poly(vinylidene fluoride-co-hexafluoropropylene) (PVDF-HFP) with the MW of ~ 400,000 g/mol, and Triethyl Phosphate (TEP) with a purity of ≥ 99% were purchased from Sigma-Aldrich; Graphene Nanoplatelets (GNP, Graphene Nano Platelets Grade 4, purity > 99%, average platelet size > 2 μm, average thickness ~ 8-15 nm, surface area ~ 500-700 m^2/g, CAS Number #7782-42-5) was purchased from Cheap Tubes Inc. Carbon Dioxide gas tank (CO_2, Coleman Instrument grade, purity > 99.99%) was acquired at Matheson Tri-Gas, Inc. The polished 6-MHz Gold AT Quartz Crystals (QC) were purchased from Phillips Tech. The Quartz Crystal Microbalance (QCM) sensor (Phoenix Temperature Monitoring Sensor System with Eon-LT Monitor) was purchased at Colnatec Inc. The silicon wafer (type P, Boron dopant (B), resistivity ~ 0.005-0.02, thickness ~ 500 μm, Virgin Test grade, the orientation of <100>, the diameter of 5.08 cm, single-side polished) was purchased from the University Wafer.

2.2. Sample preparation

Mixtures of polymers and ionic liquids with a different composition were prepared for the study of CO_2 sorption. First, a mixture of 10 wt.% PVDF-HFP in TEP was prepared. The mixture was heated to 100 °C and stirred at 400 rpm for 24 hours. Then, the solution was cooled to room temperature. The polymeric mixtures of PVDF-HFP with 10, 30, 40, 45, 50, 55 wt. % of [Emim][TF_2N] were prepared by adding a stock solution to the 6-dram capped glass vials (VWR Vials, Borosilicate Glass). Then the mixture was weighed on an analytical balance (Sartorius, MSA225P100DI Cubis Analytical Balance) and a known amount of IL was added to each solution to make the desired composition. All mixtures were stirred and heated at 310 rpm and 95 °C on a hotplate (Heidolph Inc.) for 24 hours before they were further used in an experiment. Three main mixtures, used for the sorption study, contained 10, 30, and 50 wt. % of IL in the mixture, from which the mixture of 50 wt. % was chosen for investigating the effect of graphene nanoplatelets (GNP). The mixtures containing 10, 30, 40, 45, 50, and 55 wt. % of IL were used to establish a calibration line for the composition. For a mixture of PVDF-HFP/Ionic Liquids/Graphene Nanoplatelets, first, the polymeric mixture of PVDF-HFP/GNP was prepared. Briefly, different amounts of GNP were weighed and transferred to the vials; then polymer solutions with known compositions were added. The mixtures were stirred and heated for 24 hours at 310 rpm and 95 °C, respectively. In the second step, to reach a target composition of 50 wt. % of IL, a known amount of IL was added to the vial. The mixtures were additionally stirred and heated for 24 hours at 310 rpm and 95 °C, respectively.

For thin film preparation, the solutions were heated and stirred at 95 °C and 310 rpm, respectively, for 24 hours. Spin casting of solutions was performed on various substrates, such as silicon wafers, QCM substrates, and microscope glass slides; the details of the spin coating conditions are given in Supplementary Materials, Section S1.3. Specifically, silicon wafer substrates were used for the polarized microscope and growth rate measurement, QCM substrates were used for CO_2 capture, and glass slide substrates were used for the Fourier-Transform Infrared Spectroscopy (FTIR) measurement. The substrate was first heated at 60 °C for half an hour and then left for 71.5 hours at 110 °C.

Similar to the thin film preparation, to prepare thick films, all solutions were heated and mixed at 95 °C and 310 rpm, respectively, for 24 hours. Solutions were then poured directly into aluminum-based casting wells, with 1 cm diameter and 1.5 mm depth. The

Preprints (www.preprints.org) | NOT PEER-REVIEWED | Posted: 5 October 2022 doi:10.20944/preprints202210.0047.v1

following steps were taken to cast films: the cast polymer was transferred to a heating vacuum oven, preset at 60 °C; the oven temperature was ramped to 90 °C with a ramp rate of 1.3 °C/min and the wells were left in the oven for two hours and 30 minutes. Then, the oven temperature was increased to 150 °C with a ramp rate of 1.4 °C/min and the samples were heated for 24 hours to remove the residual TEP. At this point, the oven temperature was decreased to 110 °C. It was evacuated using a rotary vane pump, and the drying process continued for another 72 hours. The samples were kept in the vacuum oven until they were used for measurement. The thick films were prepared for the X-ray Diffraction (XRD) measurement.

2.3. Characterizations

The macroscale structural variation of the films was evaluated by observing samples under an Olympus BX51 Polarizing Microscope equipped with a Mettler Toledo FP900 thermal system with a temperature range from room temperature to 375 °C. Additionally, the films' topography was evaluated using Atomic Force Microscopy (AFM). The AFM was performed using a Bruker Dimension Icon AFM in tapping mode with a range of 15 μm. The Bruker Dimension Icon AFM was operated under ambient conditions using a commercial silicon microcantilever tip on Nitride lever with a mode of ScanAsyst-Air. Both height and inphase images were obtained using a scan rate of 0.988 Hz and 512 samples/line. The degree of crystallinity of the films was evaluated by using the X-ray Diffraction (XRD) method. The XRD measurements were performed on Rigaku SmartLab (Rigaku Co., Tokyo, Japan, SmartLab).

The measurement of CO_2 absorption was conducted by using both dynamic and static methods. The dynamic method was adopted from a previous report.[21] A high-pressure chamber equipped with a quartz crystal microbalance (QCM) was used to measure gas sorption within the film through the gravimetric. The static method is a variation of pressure drop approach.[22,23] Because obtaining reliable data for IL, via dynamic approach, was challenging, we only relied on the result from the static method and compared the results against the reported data in the literature.[24]

Before each experiment, the QCM's placeholder was cleaned with acetone and purged with nitrogen gas to remove solvent residues. The test samples, spin-coated on the QCM, were weighed on an analytical balance (Sartorius, MSA225P100DI Cubis Analytical Balance), and its weight was recorded with two digits past decimal point. Then the samples were loaded into the QCM placeholder. Initially, the system was evacuated using a rotary vane pump, and the chiller's temperature was set. When the frequency of the coated film on QCM was stabilized (~3.5 hours in continuous vacuum), the frequency and temperature of the module were logged via Eon-LT software. The pressure of chamber was also recorded in LabVIEW. Then the pressure was set on the pressure regulator, and CO_2 was introduced into the system. The ranges for pressure and temperature set points were in between 50 to 250 PSI and 10 to 40 °C, respectively. For a desorption, the QCM sensor was heated at 60 °C for 20 minutes while the system was continuously evacuated.

3. Result & Discussion

The CO_2 absorption capacity in polymer-IL films were measured, and the data are presented in Figure 1 A-C: the average values for CO_2 uptake slightly decrease as we increase the IL content of the mixture; however, this trend is reversed when the IL content is above 30%. In this range, the increase in CO_2 uptake is non-linearly correlated with the IL content. For example, for a mixture of 50 wt.% IL in polymer at 200 PSI and 10 °C, the specific molar sorption is 1.18±0.06 mol/kg, while the molar sorption for polymers and IL are 0.6±0.08 and 1.28±0.08 mol/kg, respectively. Further examining the data, we note that the measured values for CO_2 sorption in polymer samples have a large uncertainty when compared with the CO_2 sorption values for samples containing IL. Given that the PVDF-HFP is a semicrystalline polymer, we attributed the standard deviation in CO_2 sorption in polymer to the polymorphism of the samples.[25] In the samples that contain [Emim][TF_2N],

Preprints (www.preprints.org) | NOT PEER-REVIEWED | Posted: 5 October 2022 doi:10.20944/preprints202210.0047.v1

which is a known plasticizer of PVDF-HFP, this variability was not pronounced. This minor variability can be attributed to the role of IL in suppressing film crystallinity. It is also reported that the addition of salts to PVDF-HFP favors the formation of one polymorph over the others, which loosely translates into having a more homogenous film, compared to the neat polymer.

To gain further insight on the effect of composition of mixture on film structure, we conducted optical microscopy. PVDF-HFP is well known for demonstrating birefringence under polarized light;[26] therefore we used a polarized microscope for this purpose. Figure 1D presents the morphology of polymeric films as a function of their compositions. As shown, a birefringence of PVDF-HFP appears the weakest compared to other samples. As the content of IL in the film increases, a stronger birefringence is apparent, and the spherulitic domains become more discernible. This change matches the data reported in the literature, and is attributed to the preferential assembly of the polymer lamellae into the edge-on configuration.[27,28] Additionally, from Figure 1D, we can see that with an increase in the concentration of IL in the film, the spherulites become larger in size. Here, IL molecules swell polymers and alter the polymer structures. Thus, larger spherulites are observed.

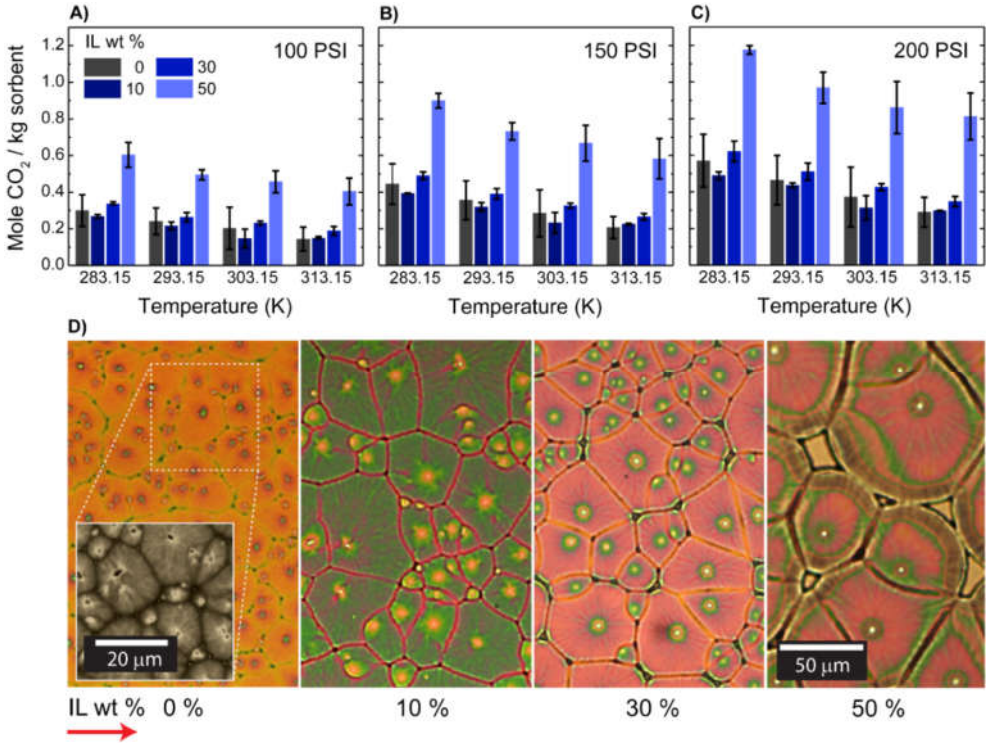

Figure 1. The effect of adding IL on the equilibrium absorption capacity of PVDF-HFP:IL mixtures at three different pressures of (A) 100, (B) 150, and (C) 200 psia. Each data point is the average of four measurements presented with one standard deviation. (D) Polarized Microscopy Images showing the spherulites grown from different mixtures with various IL content.

To further probe the film structure at a submicron level, we conducted Atomic Force Microscopy (AFM) experiments; these data are presented in Figure 2; the detail of sample preparation is described in the Supplementary Materials, Section S3.1.2. As shown in Figure 2A, the morphology of PVDF-HFP consists of dendrites composed of small short multi-branched structures, typically associated with the flat-on lamellae.[29] The lamellae originated from spherulite centers and aggregated into small fibrils in dense clusters. When the IL content was increased to 10 wt. % (Figure 2B), the dendrite-like patterns were replaced by refined and tiny fibrils. The fibrils grow parallel to each other, forming a stack of fibrils near the nuclei center. To better visualize this variation, we presented the inphase

 doi:10.20944/preprints202210.0047.v1

images in the Supplementary Materials, Figure S7. By increasing the IL content above 30 %, the tiny fibrils from the spherulites' center became omnipresent; see Figure S7. These results suggest that the addition of IL favors the formation of edge-on oriented lamellae,[28,30] leading to a transition in polymer's structures that explains the changes in the birefringence and swelling as shown in the optical images presented in Figure 1D.

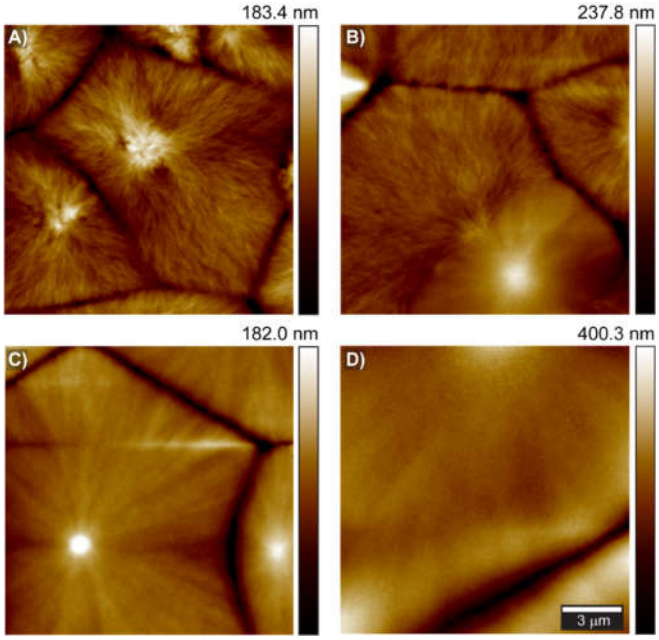

Figure 2. AFM height images of the sample spin-cast from different solutions of Polymer:IL (A) 0 wt. % IL, (B) 10 wt. % IL, (C) 30 wt. % IL, (D) 50 wt. % IL.

Motivated by the previous works on the effect of the inclusion of carbon allotropes within IL and polymer phases,[31,32] we used graphene nanoplatelets (GNP) as an additive to our mixtures and probed the variations of CO_2 uptake and film structures. For the control experiment, we chose 50 wt. % IL in polymer and to this mixture added small amount of GNP ranging between 0.1-0.4 wt. %. Figure 3A shows the CO_2 absorption capacity for different mixtures. For pressure of 100 and 200 psi, we observe a monotonic decline in the absorption capacity of the mixtures as a function of their GNP content, suggesting that CO_2 interaction with the film is weakened as the GNP content is increased. As with the Polymer/IL mixtures, we evaluated the morphology of the films under a polarized microscope to elucidate the effect of GNP content. Figure 3B (i-iv) present polarized images of samples prepared with different amount of GNP, ranging from 0 to 0.4 wt. %. The figure shows that, when GNP is added to the polymeric mixtures, the density and size of spherulitic domains is changed. This observation matches the one reported in literature.[33]

Preprints (www.preprints.org) | NOT PEER-REVIEWED | Posted: 5 October 2022 doi:10.20944/preprints202210.0047.v1

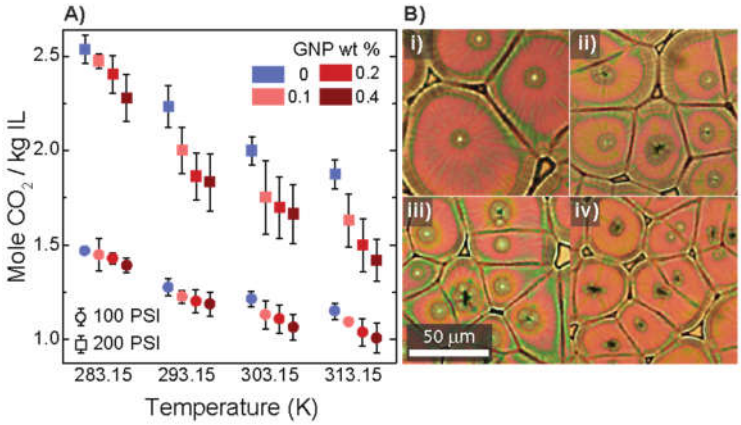

Figure 3. The effect of graphene nanoplates concentration on the properties of thin films. (A) the equilibrium absorption capacity of films at two different pressures of (⛆) 200 and (⛀) 100 psia. (B) structural variation observed under polarized microscopy. Here the concentrations of GNP are: (i) 0, (ii) 0.1, (iii) 0.2, and (iv) 0.4 wt. %. The control sample is a mixture of 50 wt. % PVDF-HFP:IL to which various amounts of GNP, as noted, are added. The error bar in Figure A represents the average values of CO_2 uptake for five different samples, presented with one standard deviation.

To establish a relationship between the structures and CO_2 absorption capacities of polymeric films, we studied the thin film's structures and properties using different characterization methods. We first look at the growth rate and average size of the spherulites grown from different mixtures. The spherulite growth rate was obtained from the slope of the plots of radii of spherulites as a function of time, which is illustrated in Figure 4A. The size of the spherulitic domains, shown in Figure 4B, was determined from the polarized optical images shown in Figure 1D and Figure 3 B-E; more details of experimental preparations and calculations are available in Supplementary Materials, Section S3.2. As shown in Figure 4A, we observe that the content of IL and GNP in the mixtures governs the growth rate and size of the spherulites. When the concentration of IL was increased to 30 wt.%, the nucleation of spherulites was delayed; increasing the IL content further to 50 wt. % shifted the onset time of the growth backward. We attributed this change to the plasticization effect of IL; the addition of IL beyond the swelling capacity of polymer [34,35] enhances the mobility of PVDF-HFP chain, while the latter leads to an enhanced nucleation rate for the spherulites.[36] In contrast, the growth rates were depreciated.

Concurrent with these changes, as shown in Figure 4A, we note that the slower growth kinetics of polymer from mixtures containing only polymer and IL leads to the formation of larger spherulites. Figures 4B and Figure 1D clearly demonstrate these changes. A reduction in the growth rate is often associated with the thermal mobility of chains, a longer time for the chains to fold into lamellae. This phenomenon facilitates branching and reduces the macroscopic growth rates.[37] Our calorimetry data, presented in Section S3.5 of Supplementary Materials, supports this point. In contrast to the Polymer/IL mixtures, for the GNP-containing mixtures, a reduction in spherulite growth rate as a function of GNP content was attributed to the existence of GNP and their agglomerates within the polymers, restraining the mobility of polymer chains. This trend has been reported for other nanocomposites.[38] When GNP was introduced to the mixtures, the required activation energy for the chains to pack from the surface significantly increased.[39] The interaction between the partial positive charge on C-H bonds of PVDF-HFP and the negative charge on the surface of GNP, creates a higher free energy barrier for nucleation, slowing down the crystallization kinetics of polymer chains.[40] However, when the GNP content was increased, the increase in the nucleation density led to the indiscriminate growth of lamellae. As a result, we observe a larger number of spherulites with smaller sizes. This behavior is in line with a previous observation.[41]

Preprints (www.preprints.org) | NOT PEER-REVIEWED | Posted: 5 October 2022 doi:10.20944/preprints202210.0047.v1

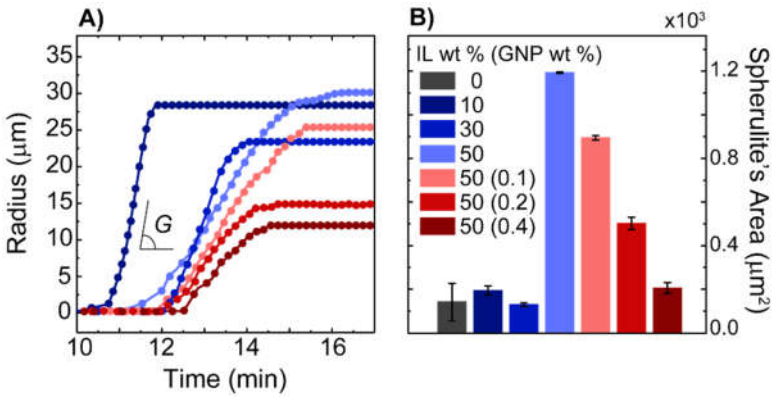

Figure 4. (A) Plot of the radii of spherulites vs. time used to estimate the spherulite growth rate (G= $\tan^{-1}$ ∡). (B) Average values for the area of spherulites; each bar is the average of three measurements, presented with one standard deviation.

To gain more information about the film composition, we analyzed the films by using Fourier-Transform Infrared Spectroscopy (FTIR) and X-ray Diffraction (XRD). Figure 5A presents a comparison of the IR spectra of polymeric films. The assignment of the vibrational bands is presented in Supplementary Materials, Section S3.3. The characteristic band at the wavenumbers of 612 and 875 cm^{-1} are assigned to the α-phase and β-phase of PVDF-HFP, respectively. Additionally, three distinct bands are assigned to SO_2 vibration of IL. The peak appears at 1348 cm^{-1}, corresponding to an antisymmetric SO_2 vibration mode of IL; it is used to estimate the IL content of the films. The procedure to estimate the composition of Polymer/IL film using FTIR signal is reported in Supplementary Materials, Section S3.3. Figure 5B presents the XRD pattern of these films; the predominant peaks at 2θ equal to ~18°, 20°, and 27°, correspond to the α-phase (020), β-phase (200), and α-phase (200) of PVDF-HFP, respectively.[41,42] The small broad peak at 38° corresponds to the α-phase (021) diffraction.[43] The peak at 27.5° represents π-π spacing of GNP;[44] this diffraction peak becomes stronger as the concentration of GNP is increased. A clear change in the diffractograms can be observed as the compositions are varied. We attributed this change in the structure of the polymer to the strong van der Waals (vdW) interaction between the imidazolium cations of IL and the negative dipoles of CF_2 groups of PVDF-HFP, controlling the crystallization kinetics and stabilizing the formation of α-phase of PVDF-HFP.[45,46]

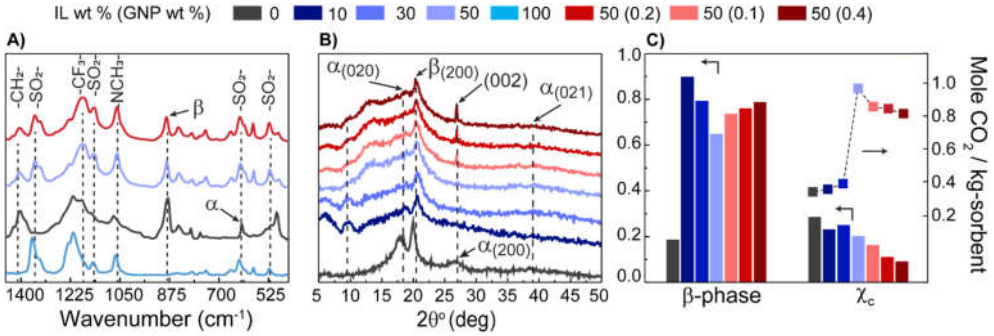

Figure 5. (A) Fourier-transform infrared spectroscopy (FTIR) fingerprint of polymer, IL, and two different mixtures cast on QCM substrate. (B) X-ray diffractograms of films cast from different mixtures. (C) The degree of β-phase and crystallinity of the samples and the normalized CO_2 absorption capacity of thin films for a sample tested at 200 psia and 313.15 K.

Additionally, we estimated the degree of crystallinity and β-phase of the films; the detailed procedures are presented in Supplementary Materials, Section S3.4. As shown in Figure 5C, increasing IL content leads to the reduction in the β-phase, which is in line with

Preprints (www.preprints.org) | NOT PEER-REVIEWED | Posted: 5 October 2022 doi:10.20944/preprints202210.0047.v1

the previous reports.[47] Furthermore, increasing the IL content enhances the flexibility of the polymer chains and results in a reduction in the degree of crystallinity of PVDF-HFP.[42] The latter can be confirmed by the broadening of the XRD peaks, an indication of an increase in the volume of the disordered domains within the film.[48,49] Notably, the addition of GNP leads to the reduction in the degree of crystallinity, but favors the formation of β-phase. Here, we expect that the interaction between partial positive charges on C-H bonds of PVDF-HFP and the negatively charged surface of GNP led to a higher probability for the formation of "all-trans" segments of PVDF-HFP.[50,51] As shown in Figure 5C, a reduction in the crystallinity of Polymer/IL films initially led to an increase in CO_2 absorption capacity of the films. Upon the addition of GNP, although the degree of crystallinity was further reduced, the trend for the CO_2 absorption was reversed. In this case, it is expected that GNP induces a variation in the dispersion of IL within the polymer matrix, weakening the solvation interactions. A similar observation dealing with GNP in complex fluid mixtures suggests that the addition of GNP weakens the interactions between the components of the mixtures.[39] Here, we think that the observed configurational changes of PVDF-HFP, due to the addition of GNP, result in an increase in the effective cohesion of IL phase through reducing Polymer/IL interaction. As a result, the CO_2 absorption in these films was decreased.

To gain more quantitative information about CO_2 sorption in the films, we estimated the enthalpies of absorption of CO_2 in polymeric films. Figure 6 presents the variation of the natural logarithm of pressure at steady states as a function of inverse temperature for 1.75 and 2.75 equivalent excess molar concentration of CO_2 (mole CO_2 per kg of IL). The isosteric enthalpies of absorption are estimated from the linear fits to the Clausius-Clapeyron equation [52] and are presented on the graph; additional data at different mole uptake are presented in Supplementary Materials, Section S2.3.3. Here, at the constant excess molar concentration of CO_2, a systematic increase in the enthalpy of absorption as a function of GNP concentration can be noted. From a design perspective, sorbents that require a higher heat of regeneration (enthalpy of absorption) and provide a lower capacity for gas absorption are not attractive;[53] however, the observed trends point to the sensitivity of the configurational properties of these mixtures to their compositions.

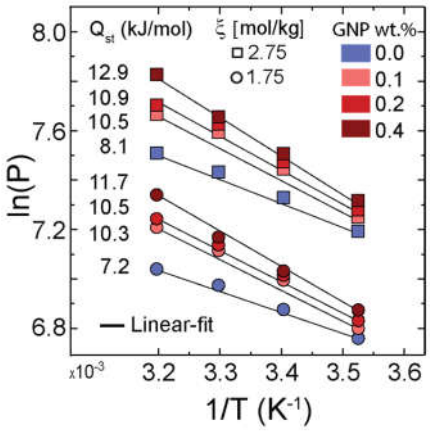

Figure 6. A linear plot of ln(P) versus 1/T at two excess molar concentrations (ξ) of (○)1.75 and (□) 2.75 mol CO_2 per kg IL; the estimated isosteric heat of absorption in kJ/mol, for each composition is reported.

4. Conclusion

In summary, we demonstrated the effects of the macrostructures of an ion gel on its CO_2 sorption capacity as a function of its composition. We observed a significant enhancement for the CO_2 sorption capacity for IL in the polymer phase. The CO_2 sorption increases nonlinearly with increasing IL content. This nonlinearity of the CO_2 sorption is not only based on the hole-filling process but is also strongly influenced by both interactions of

CO_2-Polymer/IL and the swelling behavior of polymer. Also, we observed a strong impact of an addition of a carbon allotrope; even at a small mass fraction, this addition led to a structural change at the macroscale, reducing CO_2 sorption capacity. Finally, the latter result of heat of sorption highlights the non-ideality of these mixtures and the opportunity to choose the mixture composition as a design parameter, with macroscopic fingerprints, and tune gas sorption properties of these mixtures.

Supplementary Materials: The following are available online at www.mdpi.com/xxx/s1, Figure S1-S13 and Table S1-S14.

Author Contributions: "Conceptualization, S.N. and M.B.; methodology, S.N.; software, not applicable.; validation, T.N., M.B. and S.N.; formal analysis, T.N., M.B. and S.N.; investigation, S.N. and M.B.; resources, S.N. and M.B.; data curation, S.N. and M.B.; writing—original draft preparation, S.N. and M.B.; writing—review and editing, S.N. and M.B.; visualization, S.N. and M.B.; supervision, S.N. and M.B.; project administration, S.N. and M.B.; funding acquisition, S.N. and M.B.; All authors have read and agreed to the published version of the manuscript."

Funding:

Institutional Review Board Statement: Not Applicable

Informed Consent Statement: Not Applicable

Data Availability Statement:

Conflicts of Interest: The authors declare no competing financial interest.

Acknowledgments: S. N. and T. N. thank the Nebraska Center for Energy Sciences Research (NCESR) for their generous support. The research was performed in part in the Nebraska Nanoscale Facility: National Nanotechnology Coordinated Infrastructure and the Nebraska Center for Materials and Nanoscience, which are supported by the National Science Foundation under Award ECCS: 1542182, and the Nebraska Research Initiative.

References

(1) Ueki, T.; Watanabe, M. Macromolecules in Ionic Liquids: Progress, Challenges, and Opportunities. *Macromolecules* **2008**, *41* (11), 3739–3749. https://doi.org/10.1021/ma800171k.

(2) Noro, A.; Tomita, Y.; Shinohara, Y.; Sageshima, Y.; Walish, J. J.; Matsushita, Y.; Thomas, E. L. Photonic Block Copolymer Films Swollen with an Ionic Liquid. *Macromolecules* **2014**, *47* (12), 4103–4109. https://doi.org/10.1021/ma500517e.

(3) Aoki, K.; Sugawara-Narutaki, A.; Doi, Y.; Takahashi, R. Structure and Rheology of Poly(Vinylidene Difluoride-Co-Hexafluoropropylene) in an Ionic Liquid: The Solvent Behaves as a Weak Cross-Linker through Ion–Dipole Interaction. *Macromolecules* **2022**. https://doi.org/10.1021/acs.macromol.2c00485.

(4) Yang, J.; Pruvost, S.; Livi, S.; Duchet-Rumeau, J. Understanding of Versatile and Tunable Nanostructuration of Ionic Liquids on Fluorinated Copolymer. *Macromolecules* **2015**, *48* (13), 4581–4590. https://doi.org/10.1021/acs.macromol.5b00931.

(5) Ramdin, M.; de Loos, T. W.; Vlugt, T. J. H. State-of-the-Art of CO_2 Capture with Ionic Liquids. *Ind. Eng. Chem. Res.* **2012**, *51* (24), 8149–8177. https://doi.org/10.1021/ie3003705.

(6) Pinto, A. M.; Rodríguez, H.; Arce, A.; Soto, A. Carbon Dioxide Absorption in the Ionic Liquid 1-Ethylpyridinium Ethylsulfate and in Its Mixtures with Another Ionic Liquid. *International Journal of Greenhouse Gas Control* **2013**, *18*, 296–304. https://doi.org/10.1016/j.ijggc.2013.08.005.

(7) Dai, Z.; Noble, R. D.; Gin, D. L.; Zhang, X.; Deng, L. Combination of Ionic Liquids with Membrane Technology: A New Approach for CO_2 Separation. *Journal of Membrane Science* **2016**, *497*, 1–20. https://doi.org/10.1016/j.memsci.2015.08.060.

(8) Branco, L. C.; Crespo, J. G.; Afonso, C. A. M. Highly Selective Transport of Organic Compounds by Using Supported Liquid Membranes Based on Ionic Liquids. *Angewandte Chemie International Edition* **2002**, *41* (15), 2771–2773. https://doi.org/10.1002/1521-3773(20020802)41:15<2771::AID-ANIE2771>3.0.CO;2-U.

(9) Scovazzo, P.; Visser, A. E.; Davis, J. H.; Rogers, R. D.; Koval, C. A.; DuBois, D. L.; Noble, R. D. Supported Ionic Liquid Membranes and Facilitated Ionic Liquid Membranes. In *Ionic Liquids*; ACS Symposium Series; American Chemical Society, 2002; Vol. 818, pp 69–87. https://doi.org/10.1021/bk-2002-0818.ch006.

(10) Susan, Md. A. B. H.; Kaneko, T.; Noda, A.; Watanabe, M. Ion Gels Prepared by in Situ Radical Polymerization of Vinyl Monomers in an Ionic Liquid and Their Characterization as Polymer Electrolytes. *J. Am. Chem. Soc.* **2005**, *127* (13), 4976–4983. https://doi.org/10.1021/ja045155b.

(11) Gómez, P.; Daviou, M. C.; Ibáñez, R.; Eliceche, A. M.; Ortiz, I. Comparative Behaviour of Hydrophilic Membranes in the Pervaporative Dehydration of Cyclohexane. *Journal of Membrane Science* **2006**, *279* (1), 635–644. https://doi.org/10.1016/j.memsci.2005.12.061.

(12) Wang, J.; Ding, H.; Cao, B.; Huang, X. Effect of Ionic Liquid Confinement on CO_2 Solubility and Permeability Characteristics. *Greenhouse Gases: Science and Technology* **2017**, *7* (3), 474–485. https://doi.org/10.1002/ghg.1652.

(13) Bandegi, A.; Garcia, M. M.; Bañuelos, J. L.; Firestone, M. A.; Foudazi, R. Soft Nanoconfinement of Ionic Liquids in Lyotropic Liquid Crystals. *Soft Matter* **2021**, *17* (35), 8118–8129. https://doi.org/10.1039/D1SM00796C.

(14) Pohorille, A.; Pratt, L. R. Cavities in Molecular Liquids and the Theory of Hydrophobic Solubilities. *J. Am. Chem. Soc.* **1990**, *112* (13), 5066–5074. https://doi.org/10.1021/ja00169a011.

(15) Vericella, J. J.; Baker, S. E.; Stolaroff, J. K.; Duoss, E. B.; Hardin, J. O.; Lewicki, J.; Glogowski, E.; Floyd, W. C.; Valdez, C. A.; Smith, W. L.; Satcher, J. H.; Bourcier, W. L.; Spadaccini, C. M.; Lewis, J. A.; Aines, R. D. Encapsulated Liquid Sorbents for Carbon Dioxide Capture. *Nat Commun* **2015**, *6* (1), 6124. https://doi.org/10.1038/ncomms7124.

(16) Banu, L. A.; Wang, D.; Baltus, R. E. Effect of Ionic Liquid Confinement on Gas Separation Characteristics. *Energy Fuels* **2013**, *27* (8), 4161–4166. https://doi.org/10.1021/ef302038e.

(17) Wang, J.; Ding, H.; Cao, B.; Huang, X. Effect of Ionic Liquid Confinement on CO_2 Solubility and Permeability Characteristics. *Greenhouse Gases: Science and Technology* **2017**, *7* (3), 474–485. https://doi.org/10.1002/ghg.1652.

(18) Close, J. J.; Farmer, K.; Moganty, S. S.; Baltus, R. E. CO_2/N_2 Separations Using Nanoporous Alumina-Supported Ionic Liquid Membranes: Effect of the Support on Separation Performance. *Journal of Membrane Science* **2012**, *390–391*, 201–210. https://doi.org/10.1016/j.memsci.2011.11.037.

(19) Moya, C.; Alonso-Morales, N.; Gilarranz, M. A.; Rodriguez, J. J.; Palomar, J. Encapsulated Ionic Liquids for CO_2 Capture: Using 1-Butyl-Methylimidazolium Acetate for Quick and Reversible CO_2 Chemical Absorption. *ChemPhysChem* **2016**, *17* (23), 3891–3899. https://doi.org/10.1002/cphc.201600977.

(20) Moya, C.; Alonso-Morales, N.; de Riva, J.; Morales-Collazo, O.; Brennecke, J. F.; Palomar, J. Encapsulation of Ionic Liquids with an Aprotic Heterocyclic Anion (AHA-IL) for CO_2 Capture: Preserving the Favorable Thermodynamics and Enhancing the Kinetics of Absorption. *J. Phys. Chem. B* **2018**, *122* (9), 2616–2626. https://doi.org/10.1021/acs.jpcb.7b12137.

(21) Baltus, R. E.; Culbertson, B. H.; Dai, S.; Luo, H.; DePaoli, D. W. Low-Pressure Solubility of Carbon Dioxide in Room-Temperature Ionic Liquids Measured with a Quartz Crystal Microbalance. *J. Phys. Chem. B* **2004**, *108* (2), 721–727. https://doi.org/10.1021/jp036051a.

(22) Anthony, J. L.; Maginn, E. J.; Brennecke, J. F. Solubilities and Thermodynamic Properties of Gases in the Ionic Liquid 1-n-Butyl-3-Methylimidazolium Hexafluorophosphate. *J. Phys. Chem. B* **2002**, *106* (29), 7315–7320. https://doi.org/10.1021/jp020631a.

(23) Shiflett, M. B.; Maginn, E. J. The Solubility of Gases in Ionic Liquids. *AIChE Journal* **2017**, *63* (11), 4722–4737. https://doi.org/10.1002/aic.15957.

(24) Cadena, C.; Anthony, J. L.; Shah, J. K.; Morrow, T. I.; Brennecke, J. F.; Maginn, E. J. Why Is CO_2 So Soluble in Imidazolium-Based Ionic Liquids? *J. Am. Chem. Soc.* **2004**, *126* (16), 5300–5308. https://doi.org/10.1021/ja039615x.

(25) Abbrent, S.; Plestil, J.; Hlavata, D.; Lindgren, J.; Tegenfeldt, J.; Wendsjö, Å. Crystallinity and Morphology of PVdF–HFP-Based Gel Electrolytes. *Polymer* **2001**, *42* (4), 1407–1416. https://doi.org/10.1016/S0032-3861(00)00517-6.

(26) Gozdz, A. S.; Schmutz, C. N.; Tarascon, J.-M. Rechargeable Lithium Intercalation Battery with Hybrid Polymeric Electrolyte. US5296318A, March 22, 1994.

(27) Nurkhamidah, S.; Woo, E. M. Mechanisms of Multiple Types of Lamellae and Spherulites in Poly(l-Lactic Acid) Interacting with Poly(4-Vinyl Phenol). *Macromolecular Chemistry and Physics* **2013**, *214* (20), 2345–2354. https://doi.org/10.1002/macp.201300380.

(28) Chuang, W.-T.; Hong, P.-D.; Chuah, H. H. Effects of Crystallization Behavior on Morphological Change in Poly(Trimethylene Terephthalate) Spherulites. *Polymer* **2004**, *45* (7), 2413–2425. https://doi.org/10.1016/j.polymer.2004.01.048.

(29) Jeon, K.; Krishnamoorti, R. Morphological Behavior of Thin Linear Low-Density Polyethylene Films. *Macromolecules* **2008**, *41* (19), 7131–7140. https://doi.org/10.1021/ma800652p.

(30) Liu, Y.-X.; Chen, E.-Q. Polymer Crystallization of Ultrathin Films on Solid Substrates. *Coordination Chemistry Reviews* **2010**, *254* (9), 1011–1037. https://doi.org/10.1016/j.ccr.2010.02.017.

(31) Fukushima, T.; Kosaka, A.; Ishimura, Y.; Yamamoto, T.; Takigawa, T.; Ishii, N.; Aida, T. Molecular Ordering of Organic Molten Salts Triggered by Single-Walled Carbon Nanotubes. *Science* **2003**. https://doi.org/10.1126/science.1082289.

(32) Kou, Y.; Cheng, X.; Macosko, C. W. Polymer/Graphene Composites via Spinodal Decomposition of Miscible Polymer Blends. *Macromolecules* **2019**, *52* (20), 7625–7637. https://doi.org/10.1021/acs.macromol.9b01391.

(33) Bidsorkhi, H. C.; D'Aloia, A. G.; De Bellis, G.; Proietti, A.; Rinaldi, A.; Fortunato, M.; Ballirano, P.; Bracciale, M. P.; Santarelli, M. L.; Sarto, M. S. Nucleation Effect of Unmodified Graphene Nanoplatelets on PVDF/GNP Film Composites. *Materials Today Communications* **2017**, *11*, 163–173. https://doi.org/10.1016/j.mtcomm.2017.04.001.

(34) Izák, P.; Hovorka, Š.; Bartovský, T.; Bartovská, L.; Crespo, J. G. Swelling of Polymeric Membranes in Room Temperature Ionic Liquids. *Journal of Membrane Science* **2007**, *296* (1), 131–138. https://doi.org/10.1016/j.memsci.2007.03.022.

(35) Subianto, S.; Mistry, M. K.; Choudhury, N. R.; Dutta, N. K.; Knott, R. Composite Polymer Electrolyte Containing Ionic Liquid and Functionalized Polyhedral Oligomeric Silsesquioxanes for Anhydrous PEM Applications. *ACS Appl. Mater. Interfaces* **2009**, *1* (6), 1173–1182. https://doi.org/10.1021/am900020w.

(36) Tong, F.; Xu, H.; Yu, J.; Wen, L.; Zhang, J.; He, J. Plasticization of [C12MIM][PF6] Ionic Liquid on Foaming Performance of Poly(Methyl Methacrylate) in Supercritical CO_2. *Ind. Eng. Chem. Res.* **2012**, *51* (38), 12329–12336. https://doi.org/10.1021/ie301409h.

(37) Jiang, Y.; Yan, D.-D.; Gao, X.; Han, C. C.; Jin, X.-G.; Li, L.; Wang, Y.; Chan, C.-M. Lamellar Branching of Poly(Bisphenol A-Co-Decane) Spherulites at Different Temperatures Studied by High-Temperature AFM. *Macromolecules* **2003**, *36* (10), 3652–3655. https://doi.org/10.1021/ma0341061.

(38) Waddon, A. J.; Petrovic, Z. S. Spherulite Crystallization in Poly(Ethylene Oxide)–Silica Nanocomposites. Retardation of Growth Rates through Reduced Molecular Mobility. *Polym J* **2002**, *34* (12), 876–881. https://doi.org/10.1295/polymj.34.876.

(39) Zheng, X.; Sauer, B. B.; Van Alsten, J. G.; Schwarz, S. A.; Rafailovich, M. H.; Sokolov, J.; Rubinstein, M. Reptation Dynamics of a Polymer Melt near an Attractive Solid Interface. *Phys. Rev. Lett.* **1995**, *74* (3), 407–410. https://doi.org/10.1103/PhysRevLett.74.407.

(40) Wu, Y.; Hsu, S. L.; Honeker, C.; Bravet, D. J.; Williams, D. S. The Role of Surface Charge of Nucleation Agents on the Crystallization Behavior of Poly(Vinylidene Fluoride). *J. Phys. Chem. B* **2012**, *116* (24), 7379–7388. https://doi.org/10.1021/jp3043494.

(41) Lopes, A. C.; Costa, C. M.; Tavares, C. J.; Neves, I. C.; Lanceros-Mendez, S. Nucleation of the Electroactive γ Phase and Enhancement of the Optical Transparency in Low Filler Content Poly(Vinylidene)/Clay Nanocomposites. *J. Phys. Chem. C* **2011**, *115* (37), 18076–18082. https://doi.org/10.1021/jp204513w.

(42) Sownthari, K.; Austin Suthanthiraraj, S. Preparation and Properties of a Gel Polymer Electrolyte System Based on Poly-ε-Caprolactone Containing 1-Ethyl-3-Methylimidazolium Bis(Trifluoromethylsulfonyl)Imide. *Journal of Physics and Chemistry of Solids* **2014**, *75* (6), 746–751. https://doi.org/10.1016/j.jpcs.2014.02.003.

(43) Pandey, G. P.; Agrawal, R. C.; Hashmi, S. A. Magnesium Ion-Conducting Gel Polymer Electrolytes Dispersed with Nanosized Magnesium Oxide. *Journal of Power Sources* **2009**, *190* (2), 563–572. https://doi.org/10.1016/j.jpowsour.2009.01.057.

(44) Shih, C.-J.; Vijayaraghavan, A.; Krishnan, R.; Sharma, R.; Han, J.-H.; Ham, M.-H.; Jin, Z.; Lin, S.; Paulus, G. L. C.; Reuel, N. F.; Wang, Q. H.; Blankschtein, D.; Strano, M. S. Bi- and Trilayer Graphene Solutions. *Nature Nanotech* **2011**, *6* (7), 439–445. https://doi.org/10.1038/nnano.2011.94.

(45) Hayes, R.; Warr, G. G.; Atkin, R. Structure and Nanostructure in Ionic Liquids. *Chem. Rev.* **2015**, *115* (13), 6357–6426. https://doi.org/10.1021/cr500411q.

(46) Thomas, E.; Parvathy, C.; Balachandran, N.; Bhuvaneswari, S.; Vijayalakshmi, K. P.; George, B. K. PVDF-Ionic Liquid Modified Clay Nanocomposites: Phase Changes and Shish-Kebab Structure. *Polymer* **2017**, *115*, 70–76. https://doi.org/10.1016/j.polymer.2017.03.026.

(47) Dias, J. C.; Correia, D. M.; Costa, C. M.; Ribeiro, C.; Maceiras, A.; Vilas, J. L.; Botelho, G.; de Zea Bermudez, V.; Lanceros-Mendez, S. Improved Response of Ionic Liquid-Based Bending Actuators by Tailored Interaction with the Polar Fluorinated Polymer Matrix. *Electrochimica Acta* **2019**, *296*, 598–607. https://doi.org/10.1016/j.electacta.2018.11.049.

(48) Shalu; Kumar Singh, V.; Kumar Singh, R. Development of Ion Conducting Polymer Gel Electrolyte Membranes Based on Polymer PVdF-HFP, BMIMTFSI Ionic Liquid and the Li-Salt with Improved Electrical, Thermal and Structural Properties. *Journal of Materials Chemistry C* **2015**, *3* (28), 7305–7318. https://doi.org/10.1039/C5TC00940E.

(49) Prosa, T. J.; Winokur, M. J.; Moulton, J.; Smith, P.; Heeger, A. J. X-Ray Structural Studies of Poly(3-Alkylthiophenes): An Example of an Inverse Comb. *Macromolecules* **1992**, *25* (17), 4364–4372. https://doi.org/10.1021/ma00043a019.

(50) Lopes, A. C.; Caparros, C.; Ferdov, S.; Lanceros-Mendez, S. Influence of Zeolite Structure and Chemistry on the Electrical Response and Crystallization Phase of Poly(Vinylidene Fluoride). *J Mater Sci* **2013**, *48* (5), 2199–2206. https://doi.org/10.1007/s10853-012-6995-9.

(51) Martins, P.; Caparros, C.; Gonçalves, R.; Martins, P. M.; Benelmekki, M.; Botelho, G.; Lanceros-Mendez, S. Role of Nanoparticle Surface Charge on the Nucleation of the Electroactive β-Poly(Vinylidene Fluoride) Nanocomposites for Sensor and Actuator Applications. *J. Phys. Chem. C* **2012**, *116* (29), 15790–15794. https://doi.org/10.1021/jp3038768.

 doi:10.20944/preprints202210.0047.v1

(52) Brunauer, S. Chapter VIII: The Heat of Adsorption II. In *The adsorption of gases and vapors*; H. Milford, Oxford University Press, 1943; Vol. 1, pp 218–270.

(53) Srivastava, V. C.; Mall, I. D.; Mishra, I. M. Adsorption Thermodynamics and Isosteric Heat of Adsorption of Toxic Metal Ions onto Bagasse Fly Ash (BFA) and Rice Husk Ash (RHA). *Chemical Engineering Journal* **2007**, *132* (1), 267–278. https://doi.org/10.1016/j.cej.2007.01.007.